Supplementary Information

Small Details Matter: the 2'-Hydroxyl as a Conformational Switch in RNA

Leonardo Darré[1,2], Ivan Ivani[1,2], Pablo D. Dans[1,2], Hansel Gómez[1,2], Adam Hospital[1,2] and Modesto Orozco[1,2,3]*

[1]Institute for Research in Biomedicine (IRB Barcelona), The Barcelona Institute of Science and Technology, 08028 Barcelona, Spain

[2]Joint BSC-IRB Program in Computational Biology, Institute for Research in Biomedicine, 08028 Barcelona, Spain

[3]Department of Biochemistry, Faculty of Biology, University of Barcelona, 08028 Barcelona, Spain

* Send correspondence to M.Orozco: modesto.orozco@irbbarcelona.org

Contents

Supplementary Methods 1. Database Analysis.

All the analysis of NMR or X-ray structures was done using local R scripts using the bio3D[1] libraries.

Kappa Torsion Distribution. Two datasets were used to build the kappa torsion empirical distribution: i- the "Full Dataset" which contains the current state of the PDB up to June 2016 for NMR-solved structures containing RNA (610 entries), and ii- the "Non-Redundat Dataset" which contains NMR-solved RNA structures (476 entries) proposed by Leontis et al.[2] to avoid structural redundancy available from the BGSU Structural Bioinformatics Group web page (http://rna.bgsu.edu/rna3dhub/nrlist/), see Supplementary Table 1 for further details. For the Full Dataset, all NMR models in every PDB entry were split into RNA continuous segments (two or more residues), and the kappa torsion angle was measured for every ribonucleotide within a given segment. The canonical hydrogen bond local interactions of the 2'OH group were analyzed by measuring the distance between the 2'OH hydrogen atom and the atoms: O3', O4' and O2 (pyrimidines)/N3 (purines) from the same ribonucleotide, or O5', OP1, OP2 and O4' of the ribonucleotide in 3'. In addition, non-canonical hydrogen bonds were assessed by measuring the distance between the H2' or O2' of a given ribonucleotide and O4' or H5'/H5'' of the ribonucleotide in 3', respectively. To capture the effect of the sugar conformation on the kappa torsion angle, the pucker phase was also measured using Westhof & Sundaralingam definition[3] and obtaining kappa/pucker phase pairs for each analyzed ribonucleotide. Kappa probability distributions were calculated using angle windows of 20 degrees and plotted for 3'endo and 2'endo pucker phases separately, for all bases together or split by base type. The correlation between the kappa torsion angle and the distances to local hydrogen bond acceptors/donors are shown by means of scatter plots and three density contours corresponding to points in the distance-kappa space with density equal to the average density plus one, two or four standard deviations. Finally, kappa distributions were converted to empirical free energies from the relative populations of kappa values between 0 and 360 degrees, considering windows of 20, 15, 10 and 5 degrees, using the relation: $\Delta G_{i/0}=R*T*Ln(P_i/P_0)$, where P_i and P_0 are the population of kappa values for windows i and 0, respectively. The windows [0,20], [0,15], [0,10], and [0,5] were used as reference (window 0) for each of the four striding options mentioned above. The measurement of kappa and pucker and the calculation of the empirical free energy were repeated for the Non-Redundant Dataset although in this case only specific chains and NMR models were used as suggested in the BGSU Structural Bioinformatics Group web page.

Kappa Torsion and Pucker Phase Distributions in 2'OH-ARG/LYS Contacts. Both dataset mentioned in the previous section were filtered keeping only PDB entries corresponding to protein-RNA complexes (see Supplementary Table 2). Kappa and pucker distributions were obtained for ribonucleotides with the 2'OH group in contact with the aminoacids ARG and LYS (distance between any ARG or LYS atom and the oxygen atom of the 2'OH moiety lower or equal to 4 Å). When multiple atoms from the same ARG or LYS residue were in contact with a given ribonucleotide 2'OH, the corresponding kappa/pucker pair was counted only once.

Probability of Contacts Between a Given Aminoacid and the 2'OH Group. The Full and the Non-Redundant Datasets filtered to keep only protein-RNA complexes, which contain only NMR-solved structures, were supplemented with X-ray solved protein-RNA complexes obtained from the current state of the PDB (up to June 2016) or the Leontis et al. non-redundant database, respectively, for resolutions below 2.5 Å. For both NMR/X-ray datasets, the number of contacts (distance <= 4 Å) between any amino acid atom and the 2'OH oxygen atom was counted. When multiple atoms from the same amino acid were in contact with a given ribonucleotide 2'OH, the contact was counted only once to eliminate repeated counts per amino acid. The contacts frequency per amino acid was divided by the total number of observed contacts, thus obtaining the aminoacid-2'OH interaction probability given that a contact exists.

Cluster analysis of Lys and Arg residues close to south puckering. The principal components of the Cartesian coordinates of the NZ atom (Lys) or CZ atom (Arg) were calculated for all occurrences of Lys or Arg residues within 4 Å of the O2’ atom in south puckering nucleotides in the non-redundant database. The first two principal components were used as coordinates to hierarchically cluster the position of the cationic protein side chains in space. Distance histograms between all hydrogen bond donor nitrogen atoms in Lys or Arg and the O2’, O3’, OP1, OP2 and O5’ atoms in RNA were constructed for: (i) all the considered structures containing Lys residues, (ii) all the considered structures containing Arg residues, and (iii) the two main PC-based clusters.

End to end distance measurement. To account for the difference in the conformational space of RNA compared to DNA, the end to end distance was measured for all RNA and DNA fragments in the non-redundant RNA database and all available structures in the Protein Data Bank (up to 22nd Nov 2016), respectively. This was done cutting all nucleic acid fragments into dodecamer strands (removing shorter segments) and measuring the distance between the C1’ atom of the 5’ and 3’ terminal atoms.

Supplementary Methods 2. MD Additional Details.

All classical MD simulations were run using AMBER-14 suite. TLEAP code was used for systems preparation, CPPTRAJ for post-processing and analyzing trajectories and ParmEd to modify and check topologies when needed (e.g. scale torsion angles force constants for HREMD calculations). Restraints were imposed using native AMBER algorithms or by means of the PLUMED 2.2 patch to AMBER-14. Generation of free energy profiles from umbrella sampling simulations was achieved using vFEP.[4]

Unbiased Molecular Dynamics Simulations. Microsecond long MD simulations of six RNA structures corresponding to three hairpins (PDBIDs: 1JJ2, 1Q9A and 2KOC) and three kissing loops (PDBIDs: 1BAU, 2BJ2 and 2RN1) were run using parm99 forcefield[5,6] supplemented with the bsc0[7] and chiOL3[8,9] corrections (here in called "parmbsc0chiOL3") to model the RNA. To take into account solvent model effects, two of the most widely used water models were employed, TIP3P[10] for the hairpin structures and SPC/E[11] for the kissing loops structures. In all cases a 150mM ionic environment was represented using Dang parameters[12–14] for K+ and Cl-. MD simulations were performed in the NPT ensemble using Berendsen thermostat[15] with a time constant of 5 ps^{-1} and the Berendsen barostat with a time constant of 5 ps^{-1}. Equations of motion were integrated using a time step of 2fs with the pmemd.cuda code.[16] Each system was subject to 2000 steps of energy minimization with position restraints in the solute of 25 kcal/mol, followed by 1 ns of position restrained (5 kcal/mol) thermalization in the NVT ensemble and 10 ns unrestrained equilibration in the NPT ensemble. Production MD simulations were run for 1 μs. Non-bonded direct cut-off was set to 9 Å and particle mesh Ewald[17] was used for reciprocal space calculations. All bonds involving hydrogen atoms were constrained by means of SHAKE algorithm.[18]

Hamiltonian Replica Exchange Molecular Dynamics Simulations. The conformational landscape of two tetranucleotides, rGACC and rCCCC, were explored enhancing the sampling by allowing coordinates exchange between eight replicas where all torsion angle force constants are scaled by: 1, 0.9 , 0.8, 0.7, 0.6, 0.5, 0.4, and 0.3, achieving an exchange acceptance in the range of 25-60%. rGACC initial structure was taken from an A-form portion of the *H. marismortui* ribosome crystal structure (PDBID: 3G6E, residues 2623-2626), following the same approach as Henriksen et al.[19] rCCCC initial structure was generated in a random conformation using NAB. The RNA molecule in each system was modelled using parmbsc0chiOL3, solvated using the TIP3P model[10] and neutralized with

three K+ ions using Dang parameters.[12–14] Preparation of both systems for the first set of HREMD involved 2000 steps of position restrained (25 kcal/mol) minimization, and heated during 2 ns of MD from 10-150 K (NVT and 25 kcal/mol position restraints) and from 150-300 K (NPT and 5 kcal/mol position restraints), using a time step of 1 fs. System density at 300 K and 1 Bar was relaxed in 5 ns of 2 fs time step MD in the NPT ensemble with soft position restraints (0.5 kcal/mol) further extended by 500 ps of unrestrained equilibration in NVT. Production HREMD simulations were run in the NVT ensemble at 300 K using the Langevin thermostat with a collision frequency of 2 ps^{-1} and resetting the random seed at each restart to avoid synchronization effects. A 2 fs time step was used with an exchange attempt every 1 ps. Non-bonded direct cut-off was set to 8 Å and particle mesh Ewald[17] was used for reciprocal space calculations. All bonds involving hydrogen atoms were constrained by means of SHAKE algorithm.[18] The independent second run of HREMD simulations were started from the restart structures of the first run after 500 ns, assigning new velocities and equilibrating for 1 ns in the NVT ensemble. Total simulated time for both independent runs was 1.2 μs per replica. Equations of motion were integrated using the pmemd.cuda.MPI code.

Umbrella Sampling Molecular Dynamics Simulations. Classical mechanics umbrella sampling simulations were run for the rCpC dinucleotide to obtain the kappa torsion potential of mean force in order to compare with the corresponding profiles at QM/MM level. For both systems, the solute was modelled using parmbsc0chiOL3 forcefield, solvated using TIP3P water model[10] and neutralized (rCpC) with one K+ ions using Dang parameters[12–14]. The rotation of the kappa torsion was sampled in twenty windows of 18 degrees applying a restraining potential on kappa of 35 kcal/mol. Each window initial configuration was extracted from an exploratory well tempered metadynamics[20] simulation (50 ns; initial Gaussian high of 1.2 kJ/mol; deposition period of 1ps; sigma=0.35 radians; BIASFACTOR=4, T=300 K) of the rCpC dinucleotide, and further equilibrated for 500 ps in the NPT ensemble at 300K and 1 Barr. Production data was collected for 2.5 ns of NPT molecular dynamics for each window. Restraints on beta and gamma backbone torsions, as well as on the sugar pucker were used as in the QM/MM simulations detailed below. Umbrella sampling was also used to obtain the puckering PMF for the cytosine 6 residue of a RNA fragment in complex with protein MIWI PAZ domain (PDB ID: 2XFM; model 6) for the wild type (presence of Lys 316 close to the 2'OH group of cytosine 6) and for a mutant (Lys316Ala). The RNA-protein complex was modeled using parmbsc0chiOL3KappavdW forcefield modification (RNA) and FF14SB (protein), solvated

using TIP3P water model[10] and neutralized with K+ ions using Dang parameters. [12–14] The system was subject to 2000 steps of energy minimization with position restraints on both RNA and protein of 25 kcal/mol, followed by 500 ps of position restrained (5 kcal/mol) thermalization in the NVT ensemble and 500 ps restrained (2.5 kcal/mol) equilibration in the NPT ensemble. Production MD simulations were run for 2.2 ns in the NPT ensemble, keeping the last 1.2 ns for PMF calculation. Position restraints (2.5 kcal/mol) on the RNA (except for residue 6 and atoms C5', H5', H5'', O5', P', OP1 and OP2 of residue 7) where applied to avoid gross changes in the RNA structure during the puckering transition. In the case of the wild type, potential energy walls were placed at 3 Å from O2' and OP2 atoms to keep the contact with Lys 316 during the puckering transition. Non-bonded direct cut-off was set to 8 Å and particle mesh Ewald[17] was used for reciprocal space calculations. All bonds involving hydrogen atoms were constrained by means of SHAKE algorithm.[18] The pucker transition was sampled in twelve windows of 18 degrees applying a restraining potential on the pucker phase (as defined in PLUMED 2.2[22]) of 35 kcal/mol. Calculation of the free energy profile was achieved by means of the vFEP program.[4]

Supplementary Methods 3. QM/MM Additional Details.

All QM/MM dynamics simulation were run using the interface between TERACHEM[23–26] (QM) and AMBER (MM) as implemented in AMBER-14, with a time step for the integration of the equations of motion of 1 fs. Potential energy walls (when required) and/or restraints were enforced by means of PLUMED 2.2[22] patch to AMBER-14. Calculation of the free energy profile from the umbrella sampling trajectories was achieved using vFEP.[4]

Kappa Torsion Potential of Mean Force. Umbrella sampling QM/MM simulations were run to obtain the free energy profile of the C2'O2' (kappa) torsion rotation for a cytosine nucleoside (rC) and for a cytosine dinucleotide (rCpC) in aqueous solution. The system setup was the same as per the classical umbrella sampling calculations (see previous section). In both cases the nucleic acid was treated at the quantum level BLYP/6-31G(d) while the aqueous environment (water or water plus one K^+ ion) was treated at the classical level (TIP3P[10] and Dang parameters[12–14] for ions). The rotation of the kappa torsion was sampled in twenty windows of 18 degrees applying a restraining potential on kappa of 35 kcal/mol. Each window was first equilibrated fully classically ("parmbsc0chiOL3") for 500 ps in the NPT ensemble (300 K and 1 Barr). The restart classical configurations were relaxed at the QM/MM level for 5 ps and production simulations were carried out for 40 and 25 ps for rC and rCpC, respectively. Wavefunction

SCF calculations were done in mixed precision including DFTD3 dispersion corrections.[27] In the case of the rC nucleoside, sugar pucker transitions were frequently observed affecting the sampling of the kappa rotation. Consequently, a potential energy wall as implemented in PLUMED 2.2[22] was applied to the Zx Cartesian coordinate of the ring puckering[21] (a lower wall at Zx=0.3 to maintain the 3'endo conformation or an upper wall at Zx=-0.3 to maintain the 2'endo conformation). The dinucleotide simulation maintained the 3'endo initial pucker, thus the use of walls was not required (that was not the case for the MM simulations where pucker phase restraints were needed). For both rC and rCpC, 5kcal/mol restraints on the beta and gamma backbone torsions were applied to avoid interactions with the phosphate oxygen atoms. For rC additional restraints (5kcal/mol) were also applied on epsilon backbone torsion to keep it at the standard value.

Supplementary Methods 4. Kappa Parametrization. In parm99bsc0chiOL3 the C2'O2' torsion rotation is controlled by three dihedral angles: C1'-C2'-O2'-HO2' (dihedral type: CT-CT-OH-HO), C3'-C2'-O2'-HO2' (dihedral type: CT-CT-OH-HO) and H2'-C2'-O2'-HO2' (dihedral type: H1-CT-OH-HO). To avoid affecting non-RNA OH moieties described using the current AMBER forcefield distributions, a new atom type for the O2' atom was introduced (OK) for refitting the Kappa torsion angle. The dihedral type H1-CT-OH-HO was substituted by H1-CT-OK-HO with a new set of parameters, while the dihedral type CT-CT-OH-HO was renamed CT-CT-OK-HO but keeping the original set of parameters. As in the parmbsc0 and parmbsc1 parametrization procedure, a flexible Metropolis Monte Carlo algorithm was used to fit a truncated third order Fourier series to the difference between: i- QM/MM pmf of the Kappa rotation for the rCpC dinucleotide, and ii- the corresponding pmf obtained at MM level ($parmbsc0chiOL3_{H1\text{-}CT\text{-}OK\text{-}HO=0}$). Both QM/MM and MM potentials of mean force were obtained from umbrella sampling calculations for the sugar in North conformation as described in Supplementary Methods 2 and 3 (see Supplementary Figure 7A). The obtained new parameters (see Supplementary Table 4) were tested on two tetranucleotide systems (rGACC and rCCCC) exhaustively exploring their conformational landscapes by means of Hamiltonian Replica Exchange simulations (see Supplementary Methods 2 for simulation details). In addition to the previous parametrization, a second fitting was performed considering a specific modification of the Lennard-Jones potential (increase in the sigma parameter) between the phosphate oxygen atoms and : i- the ribose O2', O3' atoms, and ii- the amine nitrogen of the base (N6 in A, N2 in G and N4 in C), herein called “parmbsc0chiOL3vdW”. This correction to the Lennard Jones potential is

based on the AMBER parameters revision for organic phosphates proposed by Steinbrecher et al,[28] which was recently shown to improve the description of RNA tetranucleotides.[29] In the present work, instead of including a general Lennard-Jones correction affecting the interaction between the phosphate oxygen atoms and all other atoms in the system, the specific terms affecting only the atoms mentioned above were corrected (see Supplementary Methods 5 section for the parmed.py script). The Kappa torsion parameters were fitted as before but using the parmbsc0chiOL3vdW$_{\text{H1-CT-OK-HO=0}}$ pmf for the MM level reference (see Supplementary Figure 7). The obtained parameters (see Supplementary Table 5) were tested again on the tetranucleotide systems (rGACC and rCCCC) and on microsecond-long unbiased MD simulations of a RNA hairpin (PDB ID: 2KOC; see Supplementary Methods 2 for simulation details).

Supplementary Methods 5. Parmed.py commands for the Lennard-Jones specific interactions modification.

```
changeLJPair @%OS @%N2 3.5958 0.17
changeLJPair @%O2 @%N2 3.5733 0.188944436
changeLJPair @%O2 @%OH 3.4703 0.210199905
changeLJPair @%OS @%OH 3.4928 0.189124298
changeLJPair @%O2 @%OK 3.4703 0.210199905
changeLJPair @%OS @%OK 3.4928 0.189124298
addLJType @O4' radius 1.6837 epsilon 0.1700
parmout OUTFILE
go
```

Supplementary Methods 6: QM/SCRF potential energy surface calculations. RNA Guanine residue 65 and protein Lys residue 32 from the RNA-protein complex structure with PDB ID 4BY9 was used as starting point to build the atomistic models used in Quantum Mechanics (QM) Potential Energy Surface (PES) calculations. This nucleotide-amino acid pair belongs to the most populated cluster (cluster A) of Lys residues within 4 Å of the O2’ atom of south puckering nucleotides (see Supplementary Figure 10). From such structure, the Guanine mono-phosphate (keeping the C5’, H5’, and H5’’ of the nucleotide at 3’, and completing the C5’ valence with a third H atom) and the methyl-ammonium group were kept for the QM calculation while the rest of the atoms where removed. Initially, a first round of QM geometry optimizations was performed restraining the sugar ring torsions ν1 and ν3 to scan the pucker North<->East<->South transition (0 to 190 in 10 degrees steps) and kappa at 216 degrees. Starting from these structures (restrained to the corresponding puckering value) further optimizations were performed restraining kappa to values ranging from 18 to 216 in steps of 18 degrees, giving a total of 240 calculations for

every PES. Additional restraints were applied to β, γ, ε, ζ and α torsions to maintain the experimental conformation of the backbone, and on χ at 190 or 230 degrees for North or South puckering values, respectively, to take into account the correlation between the puckering and the glycosidic torsion. Geometry optimizations in the presence of the methyl ammonium were initially done applying distance restraints between the nitrogen in methyl ammonium and both OP2 and O2' atoms in the nucleoside mono-phosphate. Such restraints were subsequently removed to let the position of the methyl ammonium to relax to the nearest potential energy minimum. This procedure ensured the presence of the hydrogen bonds with the phosphate and 2'OH in the complete PES scan. Geometry optimizations were done with the DL-FIND optimiser[30] implemented in the modular package ChemShell[31,32]. Turbomole 6.6[33] was used to compute energies and gradients at the QM(blyp[34,35]/def2-SVP[36,37]) level of theory and taking advantage of the Resolution-of-the-Identity (RI) approximation[36,38]. Geometry optimizations were performed using the continuum solvation model named Direct Conductor-like Screening Model for Real Solvents (DCOSMO-RS[39], as implemented in Turbomole), with a permittivity ε=78.

Supplementary Table 1. Kappa Analysis (only NMR structures).[a]

	Full Dataset	Non-redundant Dataset
Number of entries	**610 (*7518*)**[b]	**476 (*531*)**[b]
Number of analysed entries	**584 (*7256*)**[b]	**459 (*503*)**[b]
Number of analysed nucleotides	**174511**	**11212**

[a]All available NMR models were used in the PDB (10/06/2016) set analysis, while only specific models were used for the non-redundant dataset (see Supplementary Methods 1).
[b] Number of NMR models for the given set of PDB entries.

Supplementary Table 2. Kappa and pucker analysis for ribonucleotides with 2'OH in

contact (distance <=4 Å) with ARG or LYS (only NMR structures).

		Full Dataset	Non-redundant Dataset
Number of protein-RNA PDB entries available		**107 (*1709*)[a]**	**89 (*135*)[a]**
Number of protein-RNA PDB entries analysed		**107 (*1709*)[a]**	**89 (*135*)[a]**
Number of analysed nucleotides with the 2'OH in contact with:	ARG	**1756[b]**	**212[b]**
	LYS	**1647[b]**	**152[b]**

[a] Number of NMR models for the given set of PDB entries.

[b] Removing repeated kappa/pucker values due to contacts with different atoms of the same aminoacid in a given contact.

Supplementary Table 3. Protein-RNA contacts analysis.

	Full Dataset	Non-redundant Dataset
Number of available PDB entries	**514**	**319**
Number of available X-ray entries	**407**	**230 (*238*)[b]**
Number of available NMR entries	**107 (*1709*)[c]**	**89 (*135*)[c]**
Total number of available models (X-RAY+NMR)	**2116**	**373**
Number of analysed PDB entries	**500**	**307**
Total Number of analysed models (X-RAY+NMR)	**2102**	**361**
Number of analysed contacts (distance<=4Å)	**26760[a]**	**5309[a]**

[a] Removing repeated counts from different atoms of the same aminoacid in a given contact.

[b] Number of X-RAY models for the given set of PDB entries.

[c] Number of NMR models for the given set of PDB entries.

Supplementary Table 4. H1-CT-OK-HO parameters.

Torsion	$V_n/2$	Phase	Periodicity
H1-CT-OK-HO	0.482	18.8	-3
H1-CT-OK-HO	0.336	59.4	2
H1-CT-OK-HO	0.549	96.9	1

Supplementary Table 5. H1-CT-OK-HO parameters considering vdW specific corrections.

Torsion	$V_n/2$	Phase	Periodicity
H1-CT-OK-HO	0.501	0.0	-3
H1-CT-OK-HO	0.287	74.3	2
H1-CT-OK-HO	0.519	60.7	1

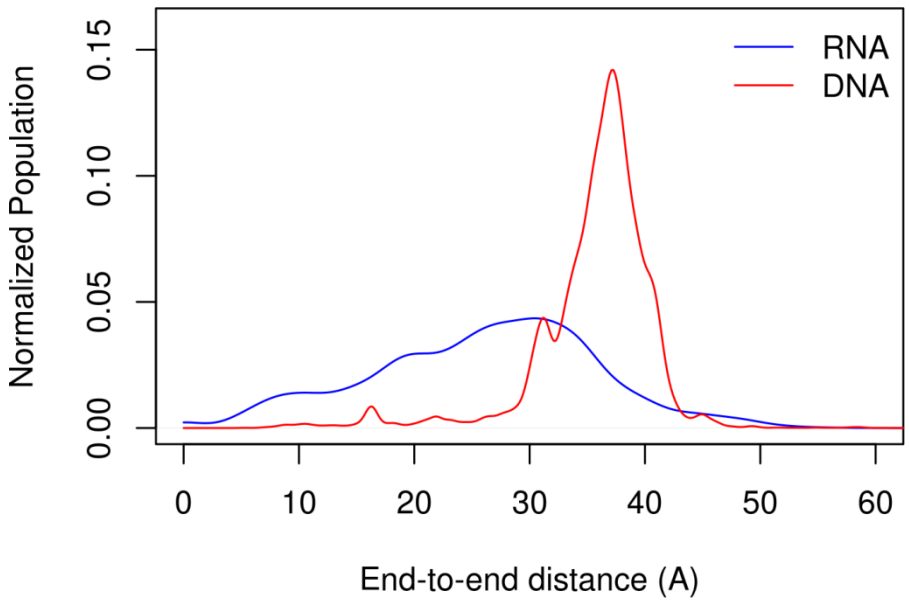

Supplementary Figure 1. End to end distance for all RNA and DNA fragments available in the non-redundant RNA database or in the Protein Data Bank (up to 22nd Nov 2016, with a filter for DNA or DNA-protein entries). Contiguous fragments of twelve residues are considered for the distance measurement discarding those shorter. The distance is defined between the C1' atoms in the 5' and 3' terminal residues.

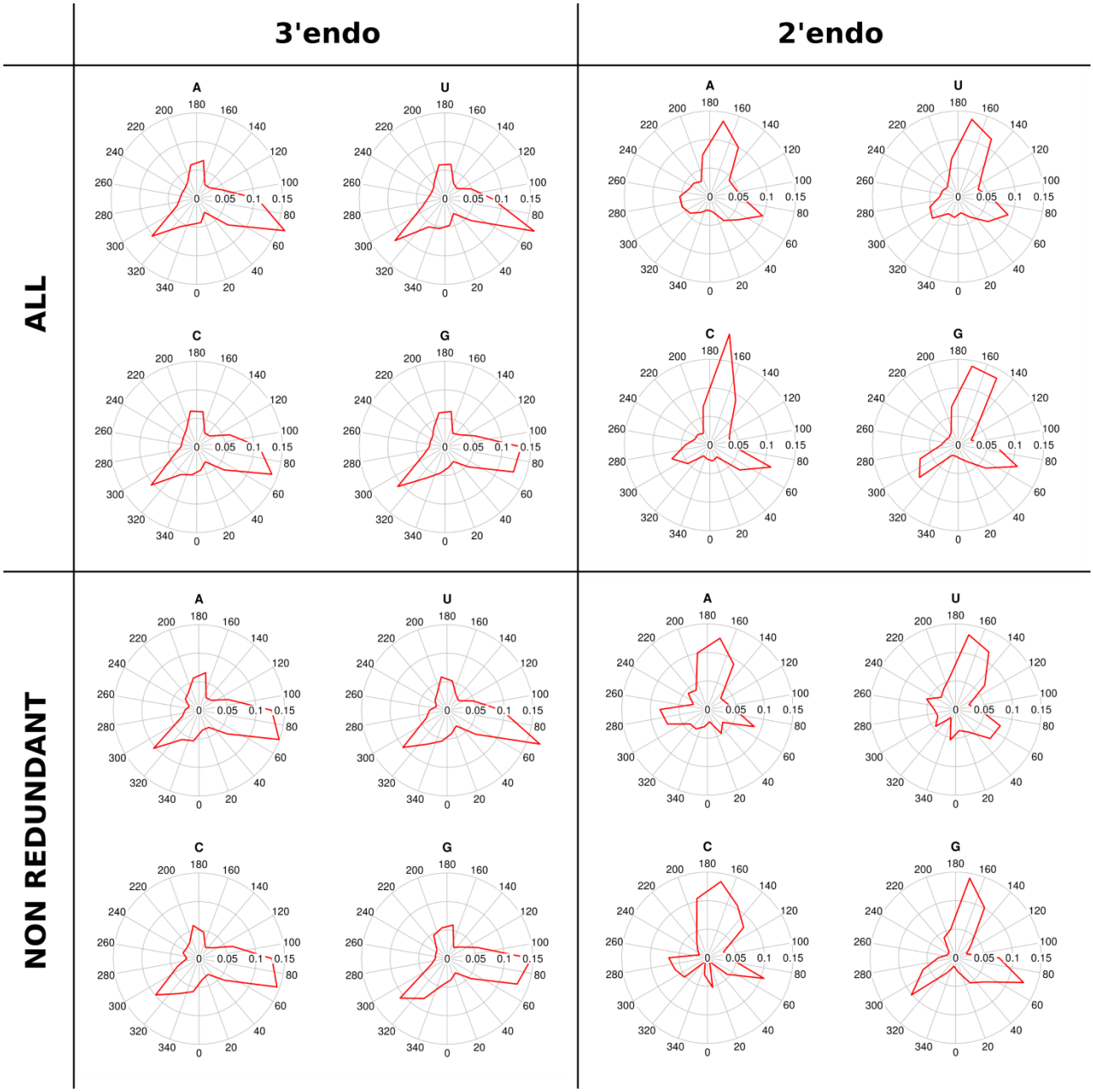

Supplementary Figure 2. Preferred orientations of the kappa torsion per base type. The plots show the probability distribution of the torsion angle between the atoms H2'-C2'-O2'-HO2' for 3'endo or 2'endo ribonucleotides and for the current state of the PDB or a non-redundant database (see Supplementary Methods 1), split by base type.

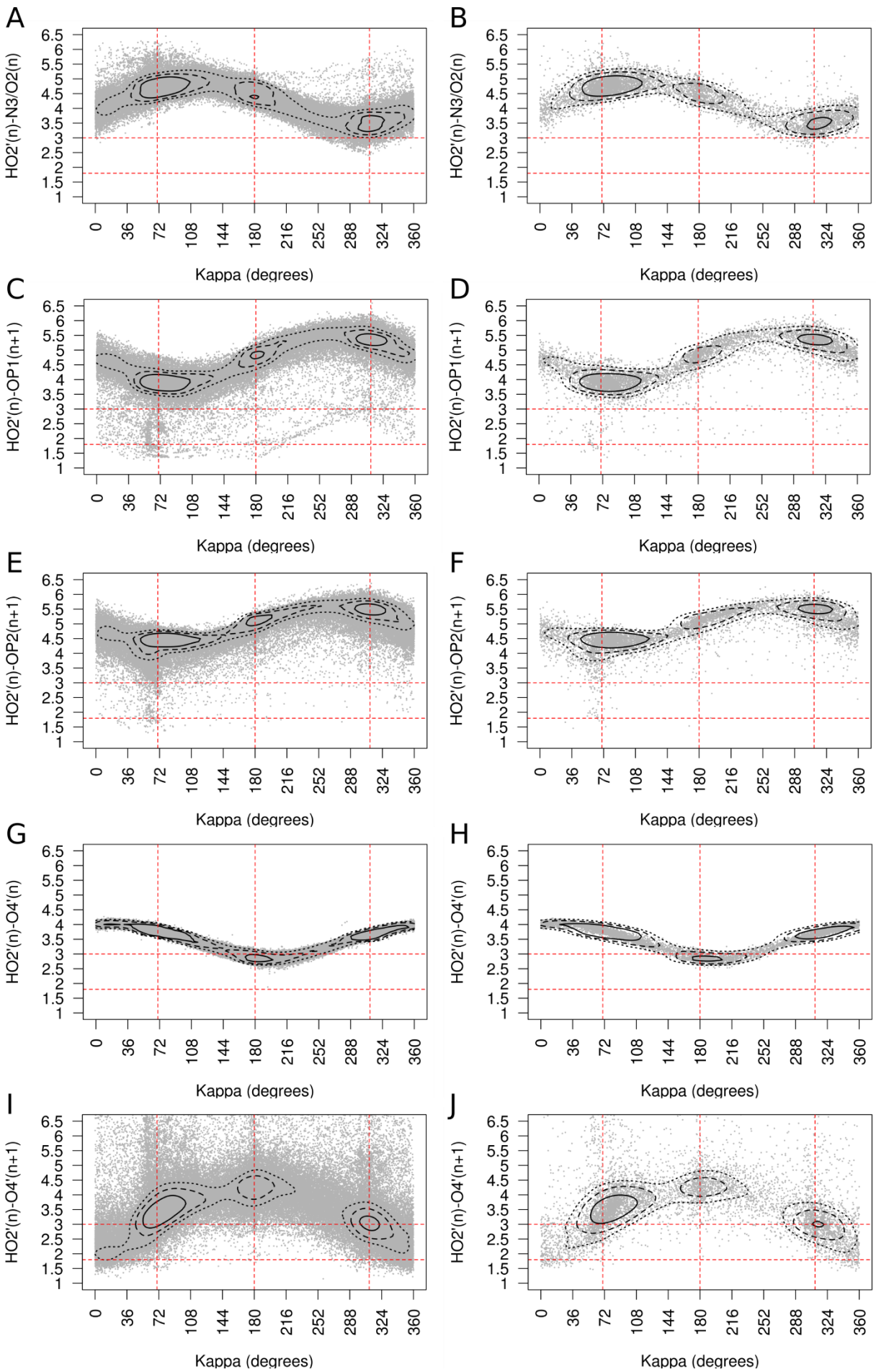
A
HO2'(n)-N3/O2(n)
B
HO2'(n)-N3/O2(n)
C
HO2'(n)-OP1(n+1)
D
HO2'(n)-OP1(n+1)
E
HO2'(n)-OP2(n+1)
F
HO2'(n)-OP2(n+1)
G
HO2'(n)-O4'(n)
H
HO2'(n)-O4'(n)
I
HO2'(n)-O4'(n+1)
J
HO2'(n)-O4'(n+1)
Kappa (degrees)
0 36 72 108 144 180 216 252 288 324 360
1 1.5 2 2.5 3 3.5 4 4.5 5 5.5 6 6.5

Supplementary Figure 3. Possible hydrogen bonds acceptor/donors nearby the 2'OH group. Scatter plots of kappa torsion vs distance between HO2' and local acceptors of hydrogen bonds, are shown for nucleotides with pucker phase in North for both Full Dataset (A, C, E, G and I) and Non-Redundant Dataset (B, D, F, H and J). Red dotted lines indicate optimal and maximum hydrogen bond distances (horizontal), and kappa rotation minimum energy positions (vertical). Contour lines correspond to points with density values equal to the average density plus 1 (dotted line), 2 (dashed line) and 4 (continuous line) standard deviations.

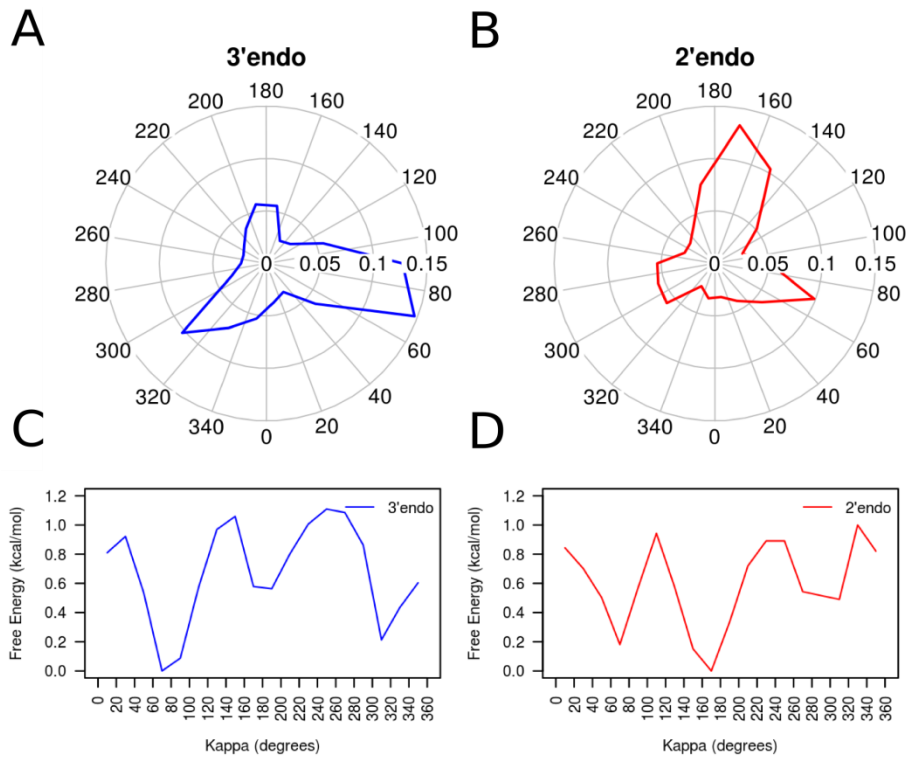

Supplementary Figure 4. Preferred orientations of the kappa torsion from a non-redundant database. (A) Probability distribution of the torsion angle between the atoms H2'-C2'-O2'-HO2' for all the 3'endo ribonucleotides of the RNA dataset obtained from a non-redundant database (see Supplementary Methods 1). (B) Same as in (A) but for 2'endo ribonucleotides. (C,D) Empirical free energy calculated from the experimental kappa distributions in (A) and (B), respectively.

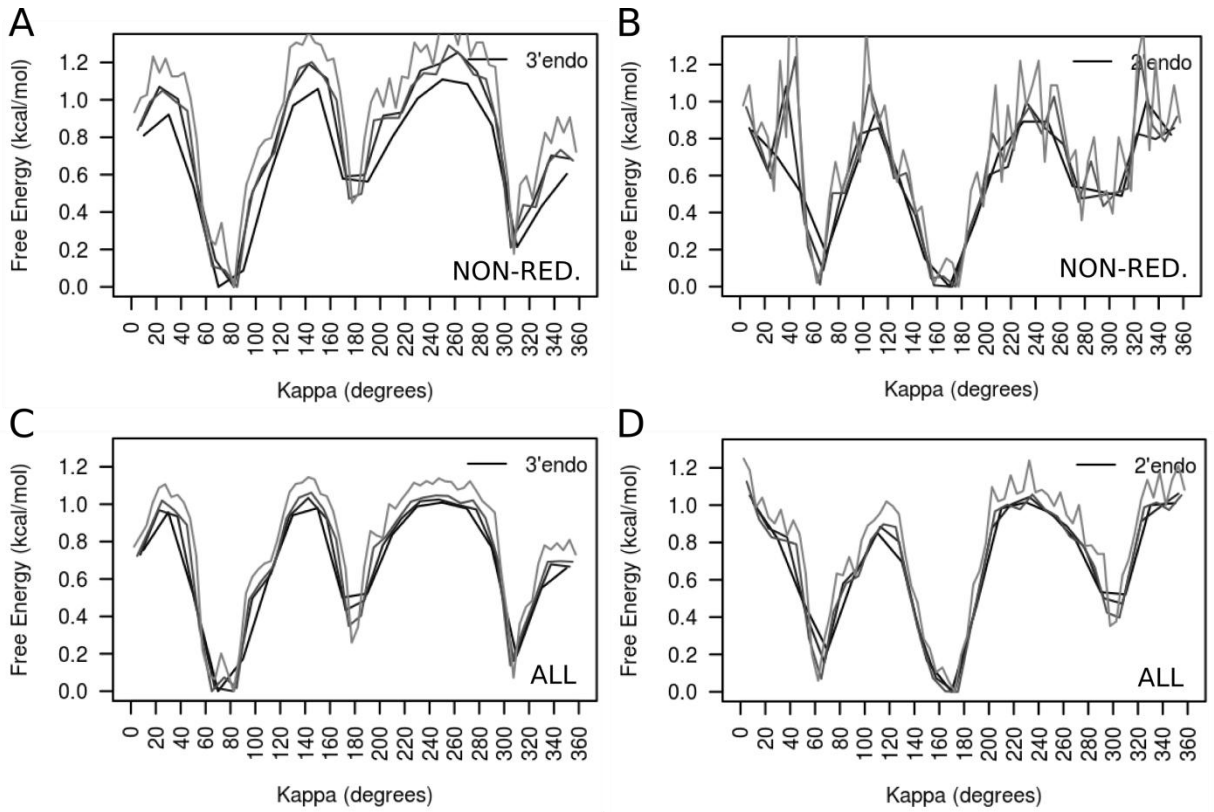

Supplementary Figure 5. Kappa energy profile for different window sizes. (A) Empirical free energy calculated from the kappa distribution of 3'endo ribonucleotides of the non-redundant RNA dataset (see Supplementary Methods 1), splitting the data using four different window sizes: 20 degress (black), 15 degrees (dark gray), 10 degrees (gray), and 5 degrees (light gray). (B) Same as in (A) but for 2'endo ribonucleotides. (C) Same as in (A) but using all current RNA entries in the PDB. (D) Same as (C) but for 2'endo ribonucleotides.

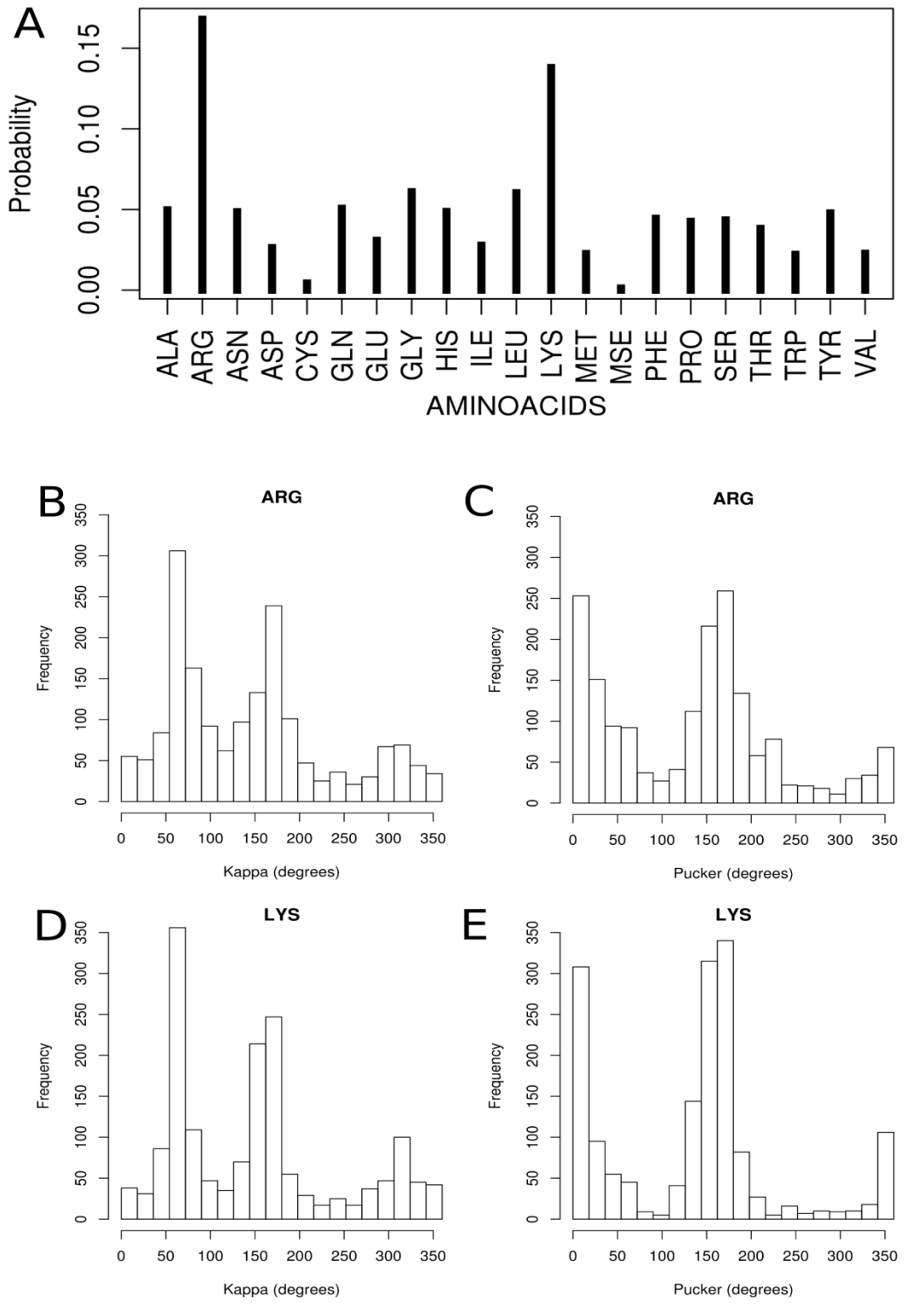

Supplementary Figure 6. Protein-RNA contacts for the Full Dataset. (A) Probability of contact between a given aminoacid and the 2'OH given a protein-RNA contact occur, calculated from counting all contacts (distance<=4 Å) between any protein atom and the oxygen of 2'OH, and splitting the counts per amino acid identity. Multiple atoms of a given aminoacid within the distance cutoff were counted as one contact. All X-ray and NMR

(multiple models) from the Full Dataset (see Supplementary Methods 1) were used. B) Frequency of kappa values for RNA nucleotides in contact with ARG atoms (distance <=4 Å) obtained from NMR (multiple models) structures in the Full dataset. C) Frequency of pucker phase values for RNA nucleotides in contact (distance <=4 Å) with ARG atoms obtained from NMR (multiple models) structures in the Full Dataset. D,E) Same as B and C, respectively, but for LYS amino acid.

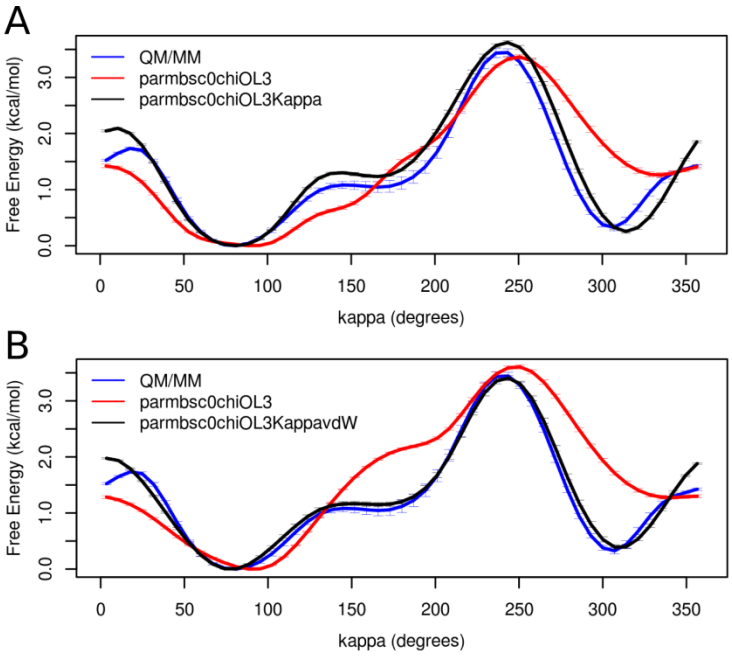

Supplementary Figure 7. Kappa fitting to reproduce QM/MM potential of mean force. (A) US QM/MM (blue), MM parmbsc0chiOL3$_{H1\text{-}CT\text{-}OK\text{-}HO=0}$ (red) and MM parmbsc0chiOL3 with the correction on the kappa torsion (parmbsc0chiOL3Kappa, black) free energy profiles for the kappa torsion of a rCC dinucleotide. The profile and error bars correspond to the average and standard deviation from five energy profiles obtained after 20-25ps every 1 ps (QM/MM) and 2-2.5ns every 100ps (parmbsc0chiOL3$_{H1\text{-}CT\text{-}OK\text{-}HO=0}$ and parmbsc0chiOL3Kappa). (B) Same as in (A) but including the Lennard-Jones modification (see Supplementary Methods 4) on parmbsc0chiOL3$_{H1\text{-}CT\text{-}OK\text{-}HO=0}$ (red) and on parmbsc0chiOL3Kappa (black).

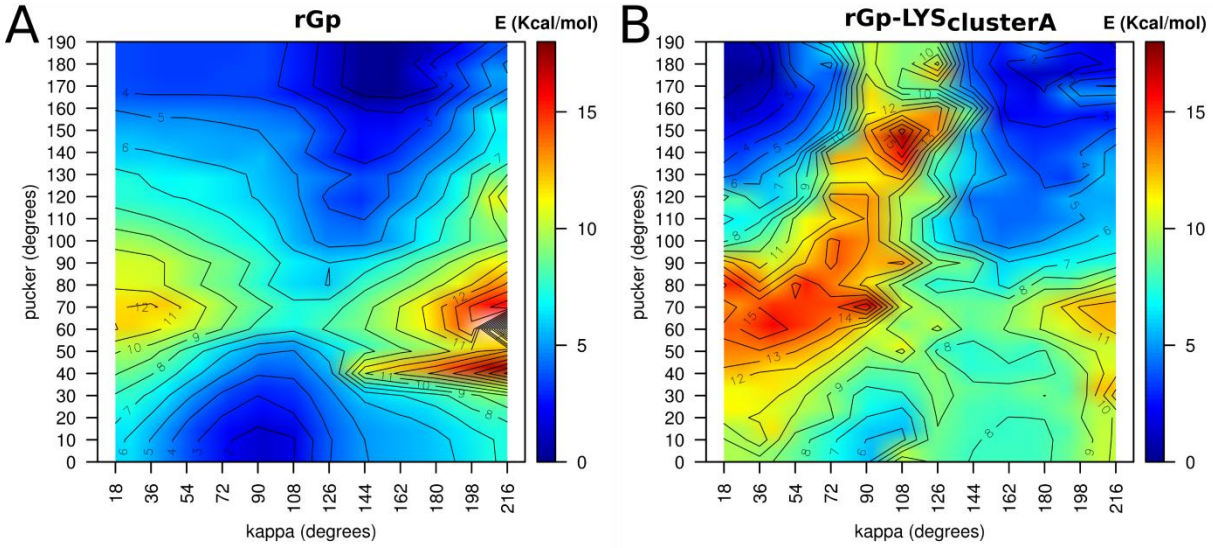

Supplementary Figure 8: κ vs puckering QM/SCRF potential energy surfaces for guanine mono-phosphate in the absence (A) and presence (B) of a lysine analogue (methyl-ammonium) placed at the most populated position (cluster A, see Supplementary Figure 10) for cationic residues nearby the 2'OH of south puckering nucleotides in the non-redundant Database.

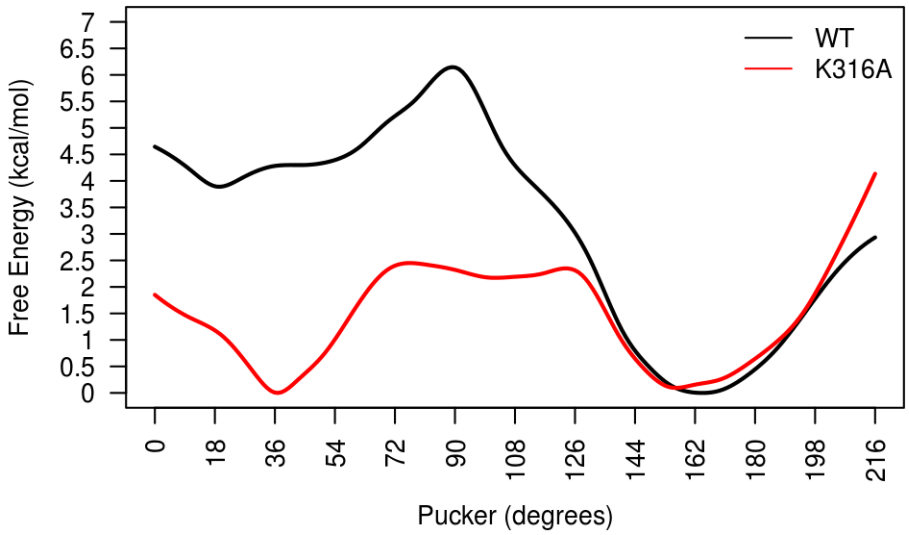

Supplementary Figure 9: Puckering PMF of cytosine 6 in the MIWI PAZ domain-RNA complex (PDB ID: 2XFM; model 6) for the wild type (black trace) where Lys 316 is located at cluster A (see Supplementary Figure 10) and for the Lys316Ala mutant.

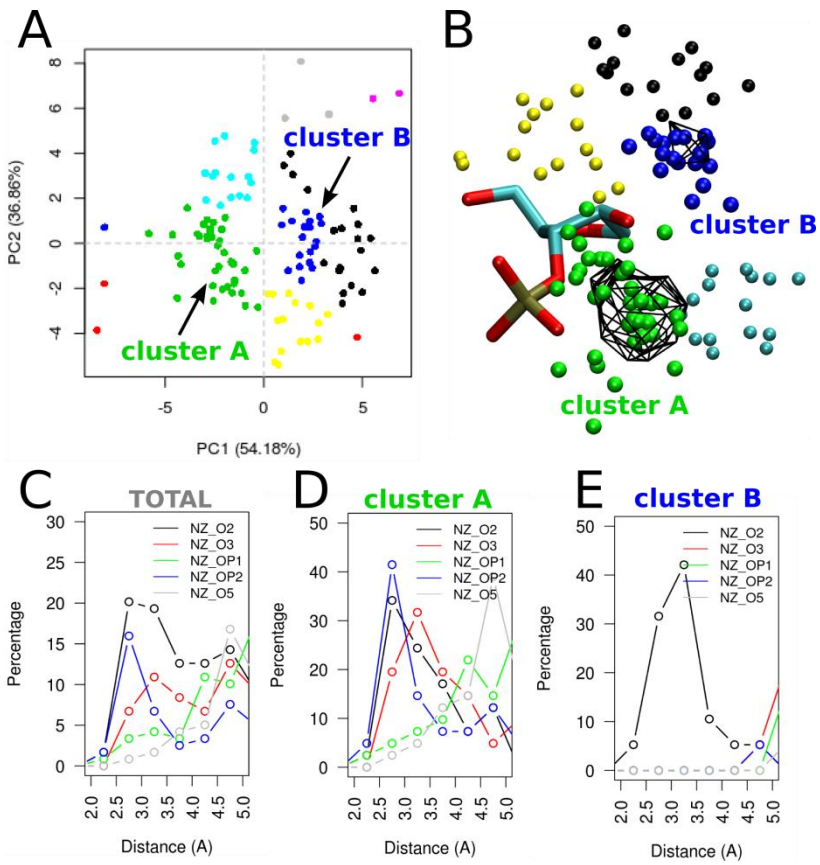

Supplementary Figure 10. Lysine localization nearby the 2'OH atom in south puckering RNA nucleotides. (A) PCA-based clustering of LYS NZ atom (projection on principal components 1 and 2) for all occurrences of LYS residues within 4 Å of the O2' of south puckering nucleotides in protein-RNA complexes of the non-redundant database. The two most populated clusters are labeled. (B) Position of the LYS ammonium atom around a nucleotide (base omitted for clarity), for the most populated clusters considered in (A), coloured by cluster identity. Occupancy isosurfaces correponding to 60% of maximum occupancy are shown as a black wireframe. (C) Histogram of the distance between NZ atom in LYS and O2', O3', OP1, OP2 and O5' in RNA for all LYS residues considered in (A). (D,E) Same as in (C) but for the two most populated clusters.

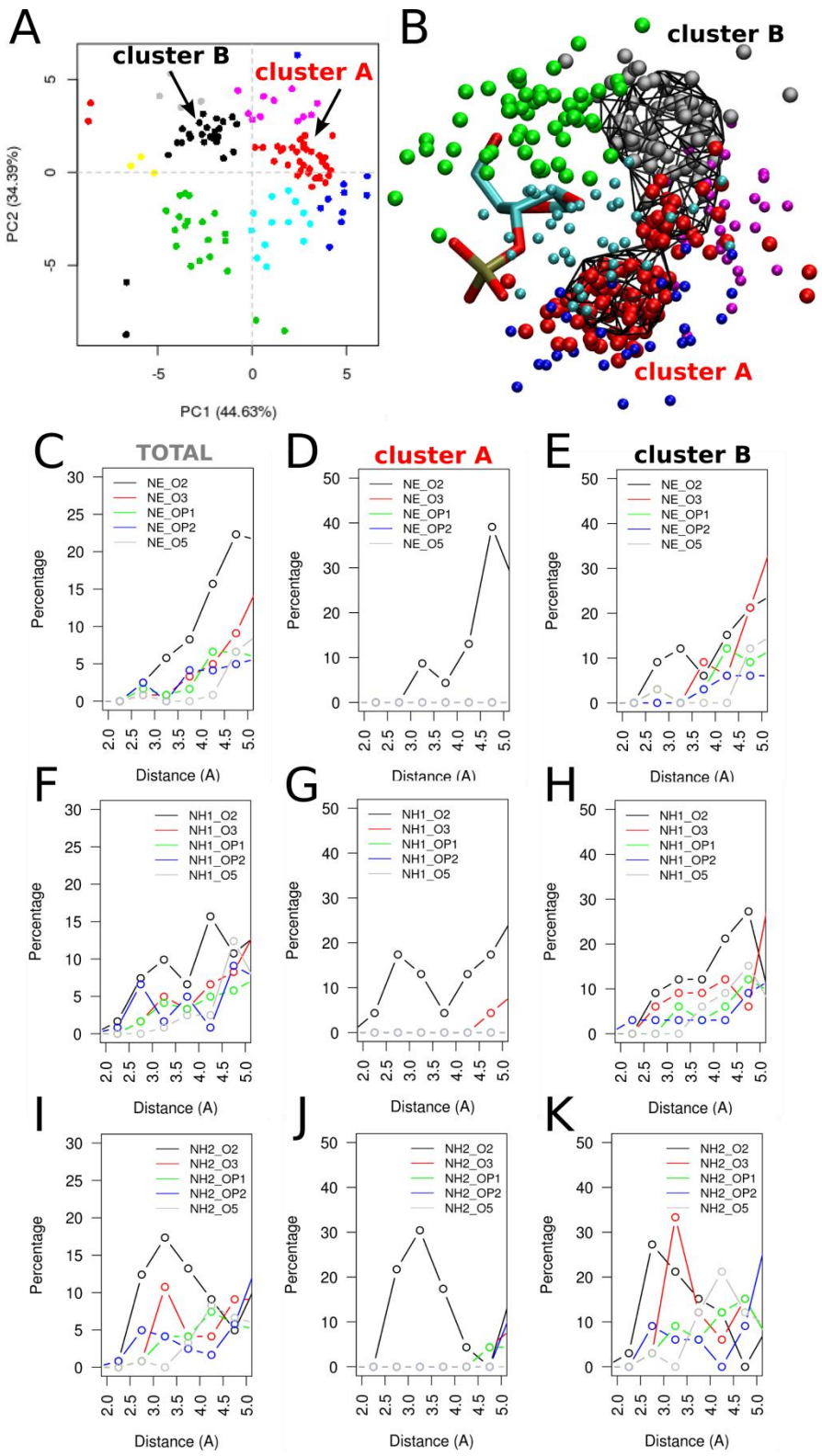

Supplementary Figure 11. Arginine localization nearby the 2'OH atom in south puckering RNA nucleotides. (A) PCA-based clustering of ARG CZ atom (projection on principal components 1 and 2) for all occurrences of ARG residues within 4 Å of the O2' of south puckering nucleotides in protein-RNA complexes of the non-redundant database. The two

most populated clusters are labeled. (B) Position of the ARG NE, NH1 and NH2 atoms around a nucleotide (base omitted for clarity), for the most populated clusters considered in (A), coloured by cluster identity. Occupancy isosurfaces correponding to 60% of maximum occupancy are shown as a black wireframe. (C) Histogram of the distance between NE atom in ARG and O2', O3', OP1, OP2 and O5' in RNA for all ARG residues considered in (A). (D,E) Same as in (C) but for the two most populated clusters. (F,I) Same as in (C) but for NH1 and NH2 atom in ARG. (G,H) Same as (F) but for the two most populated clusters. (J,K) Same as in (I) but for the two most populated clusters.

Supplementary References

1. Grant, B. J., Rodrigues, A. P. C., ElSawy, K. M., McCammon, J. A. & Caves, L. S. D. Bio3d: an R package for the comparative analysis of protein structures. *Bioinformatics* **22,** 2695–2696 (2006).
2. Leontis, N. B. & Zirbel, C. L. in *RNA 3D Structure Analysis and Prediction* (eds. Leontis, N. & Westhof, E.) **27,** 281–298 (Springer Berlin Heidelberg, 2012).
3. Westhof, E. & Sundaralingam, M. A method for the analysis of puckering disorder in five-membered rings: the relative mobilities of furanose and proline rings and their effects on polynucleotide and polypeptide backbone flexibility. *J. Am. Chem. Soc.* **105,** 970–976 (1983).
4. Lee, T.-S., Radak, B. K., Pabis, A. & York, D. M. A New Maximum Likelihood Approach for Free Energy Profile Construction from Molecular Simulations. *J. Chem. Theory Comput.* **9,** 153–164 (2013).
5. Cheatham, T. E., Cieplak, P. & Kollman, P. A. A Modified Version of the Cornell *et al.* Force Field with Improved Sugar Pucker Phases and Helical Repeat. *J. Biomol. Struct. Dyn.* **16,** 845–862 (1999).
6. Cornell, W. D. *et al.* A Second Generation Force Field for the Simulation of Proteins, Nucleic Acids, and Organic Molecules. *J. Am. Chem. Soc.* **117,** 5179–5197 (1995).
7. Pérez, A. *et al.* Refinement of the AMBER Force Field for Nucleic Acids: Improving the Description of α/γ Conformers. *Biophys. J.* **92,** 3817–3829 (2007).

8. Zgarbová, M. *et al.* Refinement of the Cornell et al. Nucleic Acids Force Field Based on Reference Quantum Chemical Calculations of Glycosidic Torsion Profiles. *J. Chem. Theory Comput.* **7,** 2886–2902 (2011).
9. Banáš, P. *et al.* Performance of Molecular Mechanics Force Fields for RNA Simulations: Stability of UUCG and GNRA Hairpins. *J. Chem. Theory Comput.* **6,** 3836–3849 (2010).
10. Jorgensen, W. L., Chandrasekhar, J., Madura, J. D., Impey, R. W. & Klein, M. L. Comparison of simple potential functions for simulating liquid water. *J. Chem. Phys.* **79,** 926 (1983).
11. Berendsen, H. J. C., Grigera, J. R. & Straatsma, T. P. The missing term in effective pair potentials. *J. Phys. Chem.* **91,** 6269–6271 (1987).
12. Dang, L. X. & Kollman, P. A. Free Energy of Association of the K+:18-Crown-6 Complex in Water: A New Molecular Dynamics Study. *J. Phys. Chem.* **99,** 55–58 (1995).
13. Dang, L. X. Mechanism and Thermodynamics of Ion Selectivity in Aqueous Solutions of 18-Crown-6 Ether: A Molecular Dynamics Study. *J. Am. Chem. Soc.* **117,** 6954–6960 (1995).
14. Smith, D. E. & Dang, L. X. Computer simulations of NaCl association in polarizable water. *J. Chem. Phys.* **100,** 3757 (1994).
15. Berendsen, H. J. C., Postma, J. P. M., van Gunsteren, W. F., DiNola, A. & Haak, J. R. Molecular dynamics with coupling to an external bath. *J. Chem. Phys.* **81,** 3684 (1984).
16. Salomon-Ferrer, R., Götz, A. W., Poole, D., Le Grand, S. & Walker, R. C. Routine Microsecond Molecular Dynamics Simulations with AMBER on GPUs. 2. Explicit Solvent Particle Mesh Ewald. *J. Chem. Theory Comput.* **9,** 3878–3888 (2013).
17. Darden, T., York, D. & Pedersen, L. Particle mesh Ewald: An N· log(N) method for Ewald sums in large systems. *J. Chem. Phys.* **98,** 10089 (1993).
18. Ryckaert, J.-P., Ciccotti, G. & Berendsen, H. J. . Numerical integration of the cartesian equations of motion of a system with constraints: molecular dynamics of n-alkanes. *J. Comput. Phys.* **23,** 327–341 (1977).

19. Henriksen, N. M., Roe, D. R. & Cheatham, T. E. Reliable Oligonucleotide Conformational Ensemble Generation in Explicit Solvent for Force Field Assessment Using Reservoir Replica Exchange Molecular Dynamics Simulations. *J. Phys. Chem. B* **117,** 4014–4027 (2013).
20. Barducci, A., Bussi, G. & Parrinello, M. Well-Tempered Metadynamics: A Smoothly Converging and Tunable Free-Energy Method. *Phys. Rev. Lett.* **100,** (2008).
21. Huang, M., Giese, T. J., Lee, T.-S. & York, D. M. Improvement of DNA and RNA Sugar Pucker Profiles from Semiempirical Quantum Methods. *J. Chem. Theory Comput.* **10,** 1538–1545 (2014).
22. Tribello, G. A., Bonomi, M., Branduardi, D., Camilloni, C. & Bussi, G. PLUMED 2: New feathers for an old bird. *Comput. Phys. Commun.* **185,** 604–613 (2014).
23. Ufimtsev, I. S. & Martinez, T. J. Quantum Chemistry on Graphical Processing Units. 3. Analytical Energy Gradients, Geometry Optimization, and First Principles Molecular Dynamics. *J. Chem. Theory Comput.* **5,** 2619–2628 (2009).
24. Titov, A. V., Ufimtsev, I. S., Luehr, N. & Martinez, T. J. Generating Efficient Quantum Chemistry Codes for Novel Architectures. *J. Chem. Theory Comput.* **9,** 213–221 (2013).
25. Götz, A. W., Clark, M. A. & Walker, R. C. An extensible interface for QM/MM molecular dynamics simulations with AMBER. *J. Comput. Chem.* **35,** 95–108 (2014).
26. Isborn, C. M., Götz, A. W., Clark, M. A., Walker, R. C. & Martínez, T. J. Electronic Absorption Spectra from MM and *ab Initio* QM/MM Molecular Dynamics: Environmental Effects on the Absorption Spectrum of Photoactive Yellow Protein. *J. Chem. Theory Comput.* **8,** 5092–5106 (2012).
27. Grimme, S., Antony, J., Ehrlich, S. & Krieg, H. A consistent and accurate ab initio parametrization of density functional dispersion correction (DFT-D) for the 94 elements H-Pu. *J. Chem. Phys.* **132,** 154104 (2010).
28. Steinbrecher, T., Latzer, J. & Case, D. A. Revised AMBER Parameters for Bioorganic Phosphates. *J. Chem. Theory Comput.* **8,** 4405–4412 (2012).
29. Bergonzo, C. & Cheatham, T. E. Improved Force Field Parameters Lead to a Better

Description of RNA Structure. *J. Chem. Theory Comput.* **11,** 3969–3972 (2015).

30. Kästner J, Carr JM, Keal TW, Thiel W, Wander A, Sherwood P: DL-FIND: An Open-Source Geometry Optimizer for Atomistic Simulations. *J. Phys. Chem. A*, **113**, 11856–11865 (2009).
31. ChemShell, a Computational Chemistry Shell, see www.chemshell.org
32. Sherwood P, de Vries AH, Guest MF, Schreckenbach G, Catlow CRA, French SA, Sokol AA, Bromley ST, Thiel W, Turner AJ, et al.: QUASI: A general purpose implementation of the QM/MM approach and its application to problems in catalysis. *J. Mol. Struct. THEOCHEM*, **632**,1–28 (2003).
33. Ahlrichs R, Bär M, Häser M, Horn H, Kölmel C: Electronic structure calculations on workstation computers: The program system turbomole. *Chem. Phys. Lett.*, **162**,165–169 (1989).
34. Becke AD: Density-functional exchange-energy approximation with correct asymptotic behavior. *Phys. Rev. A*, **38**, 3098–3100 (1988).
35. Lee, Yang, Parr: Development of the Colle-Salvetti correlation-energy formula into a functional of the electron density. *Phys. Rev. B. Condens. Matter*, **37**,785–789 (1988).
35. Eichkorn K, Weigend F, Treutler O, Ahlrichs R: Auxiliary basis sets for main row atoms and transition metals and their use to approximate Coulomb potentials. *Theor. Chem. Accounts Theory, Comput. Model. (Theoretica Chim. Acta)*, **97**,119–124 (1997).
37. Weigend F, Ahlrichs R, Weigend F, Furche F, Ahlrichs R, Leininger T, Nicklass A, Küchle W, Stoll H, Dolg M, et al.: Balanced basis sets of split valence, triple zeta valence and quadruple zeta valence quality for H to Rn: Design and assessment of accuracy. *Phys. Chem. Chem. Phys.*, **7**,3297 (2005).
38. Eichkorn K, Treutler O, Öhm H, Häser M, Ahlrichs R: Auxiliary basis sets to approximate Coulomb potentials. *Chem. Phys. Lett.*, **240**,283–290 (1995).
39. Sinnecker S, Rajendran A, Klamt A, Michael Diedenhofen § and, Frank Neese: Calculation of Solvent Shifts on Electronic g-Tensors with the Conductor-Like Screening Model (COSMO) and Its Self-Consistent Generalization to Real Solvents (Direct COSMO-RS). J. Phys. Chem. A, 110,2235–2245 (2006).